Cerebral Cortex, August 2018;28: 3017–3034

doi: 10.1093/cercor/bhy125
Advance Access Publication Date: 30 May 2018
Original Article

ORIGINAL ARTICLE

How Areal Specification Shapes the Local and Interareal Circuits in a Macaque Model of Congenital Blindness

Loïc Magrou[1], Pascal Barone[2,3], Nikola T. Markov[4], Herbert P. Killackey[5], Pascale Giroud[1], Michel Berland[1], Kenneth Knoblauch[1], Colette Dehay[1] and Henry Kennedy[1,6]

[1]Univ Lyon, Université Claude Bernard Lyon 1, Inserm, Stem Cell and Brain Research Institute U1208, 69500 Bron, France, [2]Université De Toulouse Paul Sabatier, 31062 Toulouse, France, [3]Centre De Recherche Cerveau & Cognition, CNRS, UMR 5549, 31059 Toulouse, France, [4]Princeton Neuroscience Institute and Department of Psychology, Princeton University, Princeton 08544, USA, [5]Department of Neurobiology and Behavior, University of California, Irvine, Irvine, CA 92717, USA and [6]Institute of Neuroscience, State Key Laboratory of Neuroscience, Chinese Academy of Sciences (CAS) Key Laboratory of Primate Neurobiology, CAS, Shanghai 200031, China

Address correspondence to Henry Kennedy and Colette Dehay, email: henry.kennedy@inserm.fr(H.K.), colette.dehay@inserm.fr(C.D.)

Abstract

There is little understanding of the structural underpinnings of the functional reorganization of the cortex in the congenitally blind human. Taking advantage of the extensive characterization of the macaque visual system, we examine in macaque the influence of congenital blindness resulting from the removal of the retina during in utero development. This effectively removes the normal influence of the thalamus on cortical development leading to an induced hybrid cortex (HC) combining features of primary visual and extrastriate cortex. Retrograde tracers injected in HC reveal a local, intrinsic connectivity characteristic of higher order areas and show that the HC receives a uniquely strong, purely feedforward projection from striate cortex but no ectopic inputs, except from subiculum, and entorhinal cortex. Statistical modeling of quantitative connectivity data shows that HC is relatively high in the cortical hierarchy and receives a reinforced input from ventral stream areas while the overall organization of the functional streams are conserved. The directed and weighted anophthalmic cortical graph from the present study can be used to construct dynamic and structural models. These findings show how the sensory periphery governs cortical phenotype and reveal the importance of developmental arealization for understanding the functional reorganization in congenital blindness.

Key words: vision, plasticity, primate, thalamus

Introduction

There is considerable evidence of a major functional reorganization following development in the absence of the normal input from the sensory periphery. Numerous studies have shown that the sensory periphery exerts a powerful control over cortical development. For example, experimental removal of vibrissae follicles in mice leads to the absence of the corresponding cortical barrels while supernumerary vibrissae leads to the development of additional barrels (Van der Loos and Woolsey 1973; van der Loos and Dorfl 1978). Given that such influences of the sensory periphery are time specific and differ across species suggests that they illustrate a link between development and evolution via a process termed afferent specification (Killackey 1990).

Braille reading has been shown to activate the primary visual cortex, area V1 in early blind individuals (Sadato et al. 1996; Cohen et al. 1997; Buchel et al. 1998), and congenital deafness has been shown to lead to enhanced psychophysical performance in demanding attentional tasks (Bavelier et al. 2006). While the nature of the plastic changes that underpin cross-modal compensation are not fully understood, it is generally agreed that they engage molecular and activity-dependent processes during brain development (Bavelier and Neville 2002; Ruthazer and Cline 2004).

Intriguingly, the visual cortex in congenital blindness has been observed to support higher cognitive functions including language and numerical processing (Cohen et al. 1997; Roder et al. 2002; Amedi et al. 2004; Bedny et al. 2011; Burton et al. 2012; Watkins et al. 2012; Kanjlia et al. 2016). This functional shift is hypothesized to reflect a metamodal cortical function, where computations are defined by the local network, so that following developmental deafferentation, these circuits implement higher cognitive functions by accommodating diverse, possibly innately determined, long-distance inputs (Pascual-Leone and Hamilton 2001; Sur and Leamey 2001; Merabet and Pascual-Leone 2010; Bedny 2017). If cortical areas perform specific computations regardless of their input sensory modality, then one might expect that specific cognitive functions activate anatomically similar areas in sighted and early blind individuals. There is some evidence supporting this. For example, in sighted individuals area MT is involved in visual motion processing, in the early blind MT has been shown to respond preferentially to moving auditory stimuli (Wolbers et al. 2011). Likewise, the visual word form area is activated in the blind by Braille reading (Reich et al. 2011; Striem-Amit, Cohen, et al. 2012).

In contrast to the strong evidence of functional reorganization in early blindness, the extent to which visual deprivation triggers a reorganization of the large-scale network in the cortex is still controversial (Hasson et al. 2016). Hasson and colleagues examined whole-brain networks based on cortical thickness in sighted and early blind individuals and found evidence that the congenitally blind exhibited a large-scale reorganization of anatomical networks. Whether congenital blindness modifies the pathways linking cortical areas has been investigated with MRI diffusion tensor imaging which revealed atrophy of the geniculocalcarine tract (Shimony et al. 2006) but only relatively minor changes in the corticocortical pathways of the visual system (Noppeney et al. 2005; Shimony et al. 2006; Shu et al. 2009). However, there are several studies that suggest that there are serious limitations of the accuracy of diffusion MRI tractography (Thomas et al. 2014; Reveley et al. 2015). Further, the high connectedness or density of the cortical graph in macaque means that the specificity of the cortical network is not assured by binary measures (i.e., connected vs. not connected) but via differences in the weights of interareal connections (Markov, Ercsey-Ravasz, et al. 2014). Significantly, a recent study reported that quantitative probabilistic diffusion tractography showed only a modest correlation with weighted pathways revealed by tract-tracing (Donahue et al. 2016).

Hence, it is still an open question whether the functional reorganization that is observed in congenital blindness is evidence of a cognitively pluripotent cortex that becomes manifest in the absence of ascending visual inputs (Bedny 2017), or alternatively if the observed reorganization is supported by changes in the axonal pathways interconnecting cortical areas.

In the present study, we assume a developmental approach to understanding the congenitally blind brain. How does the absence of retinal input to the brain impact on the specification of visual cortical areas? Pasko Rakic showed that bilateral removal of the eyes (enucleation) at very early stages of prenatal development in the macaque leads to an in-depth modification of the development of the visual system, which he suggested would be important for understanding certain developmental disorders in humans such as anophthalmia and microphthalmia (Rakic 1988; Rakic et al. 1991). The absence of the retina at early stages of development leads to a massive loss of neurons at postnatal stages in the lateral geniculate nucleus, thereby largely reducing the afferents to the developing visual cortex (Rakic 1988). This influential study reported that removal of the retina in the fetal macaque led to a large reduction of striate cortex, and suggested that cortex that was destined to become striate cortex assumes a default phenotype (Rakic 1988). The reduction in the numbers of thalamocortical fibers following enucleation is thought to be the cause of the modification of cortical parcellation and the formation of abnormal gyri that are observed at birth in the anophthalmic monkey (Rakic 1988; Dehay et al. 1989). Subsequently, the influence of prenatal removal of the retina in reducing the thalamic input, area extent of striate cortex and gyri formation was shown to critically depend on retinal removal being prior to embryonic day 77 (E77) (Dehay et al. 1996b). Histological examination of the cortex adjacent to the reduced striate cortex indeed confirmed that it consisted of a phenotypically hybrid cortex (HC), exhibiting the combined histological and histochemical features of striate and extrastriate cortex (Dehay et al. 1996b).

Rakic speculated that the formation of a HC in the anophthalmic monkey raises profound issues about arealization of the cerebral cortex in primates and that it is an expression of the mismatch between intrinsic and extrinsic specification mechanisms (Rakic 1988). Such mismatches during evolution could occur as a result of changing body size and constitute a process leading to the creation of new cortical areas (Rakic 1988; Dehay et al. 1989; Kennedy and Dehay 1993a; Eagleson et al. 1997; Krubitzer and Seelke 2012). More precisely, the heterogeneous nature of the HC provides insight into the complementary role of intrinsic and extrinsic control of cortical development.

In other words, thalamic input to the developing cortex contributes to the formation of cortical areas in terms of their dimensions (and therefore the numbers of neurons generated) and the expression of their phenotype (which includes specifying the connectivity of the constituent neurons). There is evidence that thalamic fibers release a mitogenic factor that induces important changes in the cell-cycle control of cortical precursors (Dehay et al. 2001), which could be the expression of a general property of developing projections to modulate

neurogenesis in their targets (Kollros and Thiesse 1988; Selleck et al. 1992). Cell-cycle control and fate determination are interlinked (Cremisi et al. 2003; Shen et al. 2006), and there is considerable evidence that modulation of the cell cycle leads to the spatial and temporal changes in rates of neuron production that determines the laminar differences in neuron number leading to the characteristic cytoarchitecture of individual cortical areas (Dehay et al. 1993; Eagleson et al. 1997; Polleux et al. 1997, 1998). The role of thalamic projections in arealization would seem to be enhanced in primates given the evidence suggesting relatively normal arealization in rodent in the absence of thalamic innervation (Miyashita-Lin et al. 1999; Chou et al. 2013).

These early experiments on the consequences of bilateral removal of the retina became subsequently comprehensible in the light of research showing that patterning of the developing mammalian neocortex is consequent to an interplay between, on the one hand, the intrinsic genetic mechanisms based on morphogens and secreted signaling molecules and, on the other, the extrinsic inputs relayed to the cortex by thalamocortical axons (O'Leary and Nakagawa 2002). The small number of genes that have persistent expression across cortical development indicates a large potential for extrinsic shaping of the cortex (Bakken et al. 2016). The role of thalamic fibers in arealization is seen increasingly to be a multistep hierarchical process involving events at progenitor and neuronal levels (Alfano et al. 2014; Zembrzycki et al. 2015). The specification of layer 4 neuron identity and its experimental manipulation has been used to derive intermediate genetic features and derive a hybrid character in mouse somatosensory cortex (Pouchelon et al. 2014).

The present study investigates the cortical networks of the anophthalmic macaque visual system using a connectomic approach, employing retrograde tracers and quantification of interareal connection weights. This approach has previously allowed the development of an extensive database in the normal macaque (Markov, Ercsey-Ravasz, et al. 2014) that has proved to be a highly valuable resource for establishing structural and dynamic models of the cortex (Ercsey-Ravasz et al. 2013; Bastos et al. 2015; Chaudhuri et al. 2015; Michalareas et al. 2016). A major aim of the present study was to acquire similar resource data in the anophthalmic to open up future computational modeling in brain circuits following extensive developmental remodeling.

It is now clearly established that individual cortical areas have unique connectivity profiles, receiving a wide range of connection strengths spanning 5 orders of magnitude from 50 to 80 cortical areas (in an atlas of 91 areas) and showing remarkable interindividual consistency (Markov et al. 2011; Markov, Ercsey-Ravasz, et al. 2014). This weighted and directed database provides a valuable resource for assessing connectivity changes following enucleation. However, the fact that nearly two-thirds of the possible interareal connections actually exist, means that detection of changes in connectivity require accurate assessment of connection weights. In the present study, anophthalmic macaques received retrograde tracer injections in HC, as well as areas V2 and V4 postnatally. The findings from these experiments were compared with results following injections in V1, V2, and V4 in normal controls. This revealed, firstly that there is a 6-fold expansion of the spatial extent of local connectivity in the HC, so that the intrinsic connectivity of the HC extended over 12 mm compared with 2 mm found in area V1 in the normal brain. Secondly, HC a surprisingly high location of the HC in the cortical hierarchy as derived from a computational modeling (Markov, Vezoli, et al. 2014). In the anophthalmic we found inputs to the HC from subiculum and entorhinal cortex. Outside of these 2 areas, the set of areas projecting to the HC, areas V2 and V4 does not differ from that of normal adult controls. However, there is a highly significant increase in the relative cumulative weight of the ventral stream areas input to the early visual areas. These findings show that although HC occupies the territory that would have become primary visual cortex it exhibits features of a higher order area, thus, reflecting a combination of intrinsic and extrinsic factors on cortical specification. Understanding the interaction of these contributing factors will shed light on cortical plasticity during primate development and the neurobiology of blindness.

Materials and Methods

There were 3 experimental animals, in which we made a fast blue (FB) and a dyamidino yellow (DY) injection in each, and we compared the results to total of 10 injections made in 8 adult controls.

Anesthesia and Surgery

The present study is based on observations following bilateral enucleation performed in 3 monkey fetuses and contrasted to 8 normal controls. The enucleated fetuses were carried to term and after birth injected with retrograde tracers (DY and FB) at different postnatal ages (Table S1). Pregnant cynomolgus monkeys (Macaca fascicularis) received atropine (1.25 mg, i.m.), dexamethasone (4 mg, i.m.), isoxsuprine (2.5 mg, i.m.), and chlorpromazine (2 mg/kg, i.m.) surgical premedication. They were prepared for surgery under ketamine hydrochloride (20 mg/kg, i.m.) anesthesia. Following intubation, anesthesia was continued with 1–2% halothane in a N_2O/O_2 mixture (70/30). The heart rate was monitored, and the expired CO_2 maintained between 4.5% and 6%. Body temperature was maintained using a thermostatically controlled heating blanket. Between embryonic day 58 (E58) and E73 and using sterile procedures a midline abdominal incision was made, and uterotomy was performed (see Table S1). Enucleation (3 cases): the fetal head was exposed, bilateral eye removal performed. After these procedures the fetus was replaced in the uterus after closing the incisions. The mother was returned to her cage and given an analgesic (visceralgine, 1.25 mg, i.m.) twice daily for 2 days.

Injections of Retrograde Tracers

Identical medication, anesthesia, and monitoring procedures were used as described above. Tracer injections were placed in the HC, area V2, and area V4. Injections were made by means of Hamilton syringes in a stereotypic fashion with similar volumes ranging from 0.4 to 0.8 µL. The published changes in sulci patterns following early enucleation serving as a guide for injection placement (Dehay et al. 1996b). Following injections, artificial dura mater was applied, the bone flaps were closed, cemented and the scalp stitched back into position.

The tracer injection sites are shown in Figure 1. Three injections are located in the HC (top 3 rows in Fig. 1), 1 in area V2 (fourth row Fig. 1), and 2 in area V4 (last row Fig. 1). All injections in the enucleate brain were confined to the cortical grey matter. BB122 LH DY injection in the HC was very small and restricted to upper layers. Side-by-side injections in target areas

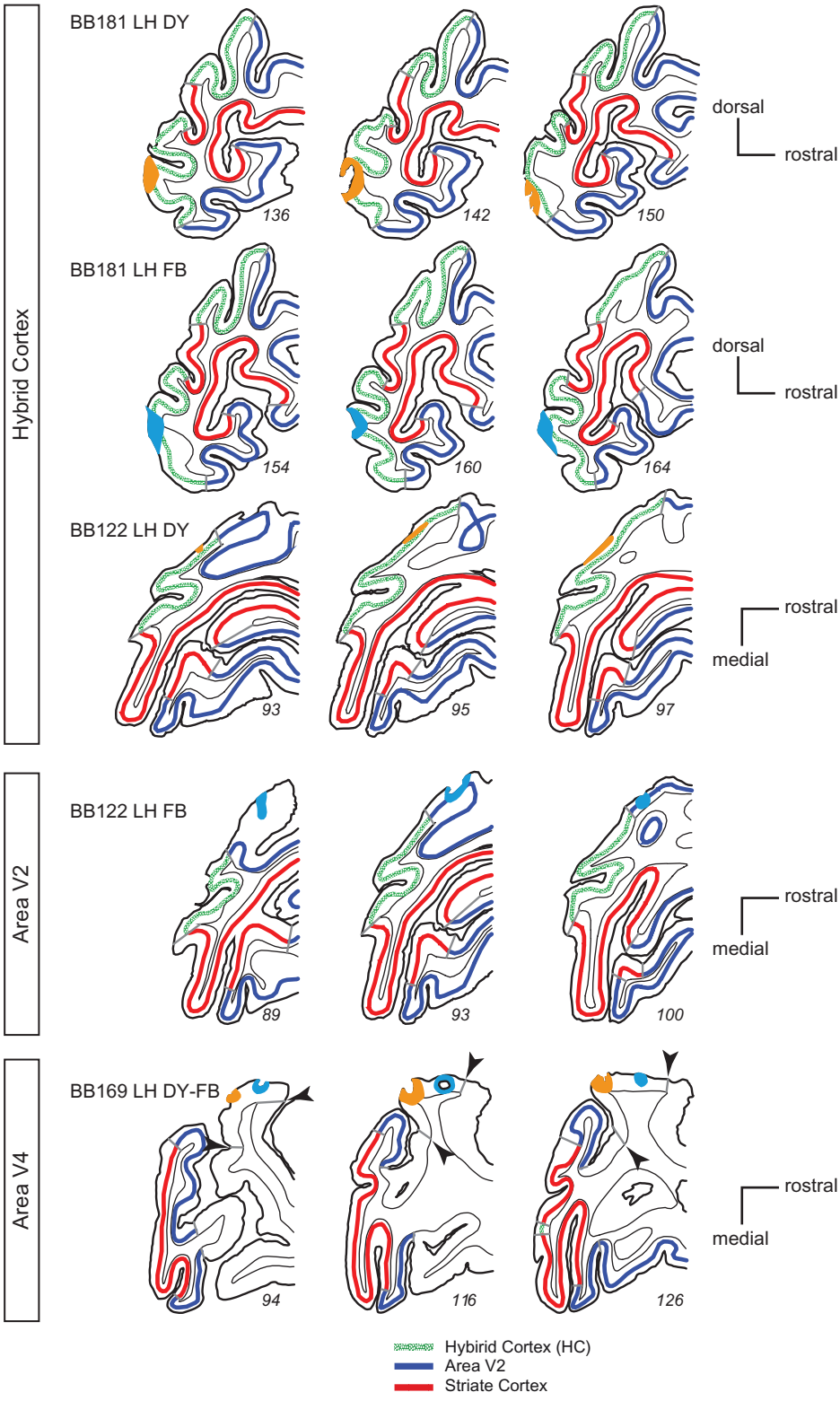

Figure 1. Location of injection sites in hybrid cortex, V2, and V4 in enucleate monkeys. Extent of the pick-up zone for the 6 injections in postal monkeys that underwent early prenatal enucleation; pick-up zones: light blue, fast blue; orange, diamidino yellow.

of retrograde tracers reveal the topology of connectivity in source areas. Such side-by-side injections were made in the HC in the lower part of the medial operculum in case BB181 corresponding in normal cortex to area V1 subserving parafoveal visual field (Gattass et al. 1987). In case BB122 a single injection was made in V2 near the lip of the lunate sulcus where foveal visual field is represented in the normal cortex (Gattass et al. 1981). Finally, a pair of large injections were made on the dorsal

part of the prelunate gyrus spanning the central and peripheral representation of area V4 in the normal brain (Li et al. 1989).

The full extent of labeled neurons were charted across the cortex, which was parcellated according to a 91 area atlas (Markov, Ercsey-Ravasz, et al. 2014). Injection of retrograde tracer in an area leads to a region of labeling in each afferent area. This region is referred to as the projection zone. So as to obtain reliable counts of labeled neurons it is necessary to chart labeled neurons throughout the full extent of the projection zone in each area (Barone et al. 1995; Markov, Vezoli, et al. 2014). This makes it possible to estimate the fraction of labeled neurons (FLN) and the fraction of supragranular layer neurons (SLN) in each area (Fig. 2A–C). As previously defined (Markov et al. 2011), the FLN is the proportion of cells located in a given source area with respect to the total number of labeled neurons in the cortex. The connectivity profile is defined by the FLN values for each of the structures labeled from the injected target area. The SLN measurement of the proportion of SLN in an area has been shown to be a stable anatomical measure of areal hierarchical relationships (Barone et al. 2000; Markov, Vezoli, et al. 2014). FLN is a weight index which allows construction of a weighted and directed matrix of the cortical network (Markov et al. 2011), while SLN values of interareal pathways constitute an index of hierarchical distance, allowing areas to be organized in a determinate hierarchy (Markov, Vezoli, et al. 2014).

Animal Euthanasia

After 10–12 days of recovery that allows optimal retrograde labeling of neurons projecting to the pick-up zone, animals were anesthetized with ketamine (20 mg/kg, i.m.) followed by a lethal dose of Nembutal (60 mg/kg, i.p.) and perfused through the heart with a 1.25% paraformaldehyde and 1.5% glutaraldehyde solution. After fixation, perfusion was continued with a 10–30% sucrose solution to provide cryoprotection of the brain.

Data Acquisition

Depending in the enucleation case, parasagittal (BB181) or horizontal (BB122 and BB169) sections (40-μm thick) were cut on a freezing microtome and at least 1 in 3 sections were stained for Nissl substance. Normal controls were cut in horizontal and coronal planes. Sections were observed in UV light with oil-immersion objectives using a Leitz fluorescence microscope equipped with a D-filter set (355–425 nm). High precision maps were made using Mercator software running on ExploraNova technology, coupled to the microscope stage. Controlled high frequency sampling gives stable neuron counts despite curvature of the cortex and heterogeneity of neuron distribution in the projection zones of individual areas (Vezoli et al. 2004; Markov, Vezoli, et al. 2014) Characteristics of neurons labeled with FB or DY are described by Keizer et al. (1983). Area limits and layer 4 were marked on the charts of labeled neurons. These neurons were then attributed to areas of our atlas based on landmarks and histology, and counted according to that parcellation (Markov, Ercsey-Ravasz, et al. 2014).

Statistical Analysis

All statistical analyses were performed in the R statistical environment (R Development Core Team 2016) with additional tools from the MASS, aods3, and betareg packages (Venables and Ripley 2002; Cribari-Neto and Zeileis 2010; Lesnoff and Lancelot 2012). Each injection gave rise to retrogradely labeled neurons, which were plotted and compared against those of normal animals, injected at anatomically equivalent locations.

Fraction of Labeled Neurons

The distribution of FLN values has been successfully modeled previously by a negative binomial distribution (Markov et al. 2011; Markov, Ercsey-Ravasz, et al. 2014). This can be performed using a generalized linear model (GLM) when the dispersion parameter is fixed. We initially estimated the dispersion parameter for individual areas obtaining values between 2.2 and 7.2, and for subsequent tests used an average value of 4. We then used this model to compare connection strengths (i.e., FLN values) between normal (i.e., nonenucleated) and enucleated animals. As explanatory variables, we used a 2-level factor, Group (normal/enclueated) and a 2-level factor, area for the labeled areas projecting on the target injection. The linear predictor in the GLM includes the main effects of both factors and their interaction. In the model, the raw neuron counts enter as the response variable, but a log link is used with the natural log of the total number of labeled neurons in each case included as a fixed offset. In this way, the model coefficients estimate FLN values. The 95% confidence intervals were computed to assess the significance of differences, based on the model fitted estimates. To test the effect of enucleation in either stream, the linear predictor was modified to include the factor group and the 2-level factor, stream (ventral/dorsal).

Supragranular Labeled Neurons

A similar approach was used to analyze SLNs (the proportion of labeled neurons situated above the layer 4 [granular layer] vs. below it, in each area) but using beta regression (Cribari-Neto and Zeileis 2010) to model the proportions. Since the beta distribution is defined on values in the interval (0, 1), it is useful for analyzing proportions. Like the binomial, the parameters of interest are linked to the explanatory values via a linear predictor. In this case a logit link was used. Like the negative binomial distribution on counts, the model includes a dispersion parameter that can account for over dispersion beyond that expected from a purely binomial process. As before, 95% confidence intervals were evaluated for the differences and significance was assessed using likelihood ratio tests.

Results

Effects of Enucleation on Areal Dimension and Local Connectivity

The 3 anophthalmics used in this study each showed important shifts in the border of striate cortex (area V1) leading to an important reduction in its dimensions (Fig. 2). In these animals, instead of the typical border between areas V1 and V2, one can detect a large region of interceding cortex where the stria of Genari is absent and its cytoarchitecture can be broadly defined as extrastriate as described in detail in earlier publications (Dehay et al. 1996a). This stretch of cortex exhibits small islands of striate cortex and the hybrid expression of histochemical phenotypes of striate and extrastriate cortex both during in utero development and postnatally (Dehay et al. 1996a, 1996b). The cortex between area V2 and the reduced striate cortex area V1 corresponds to the HC (right-hand panels of Fig. 2D,E). The proportion of area V1 with respect to the total cortex is considerably reduced in anophthalmic brains compared with the normal (Fig. 2F). This contrasts with the

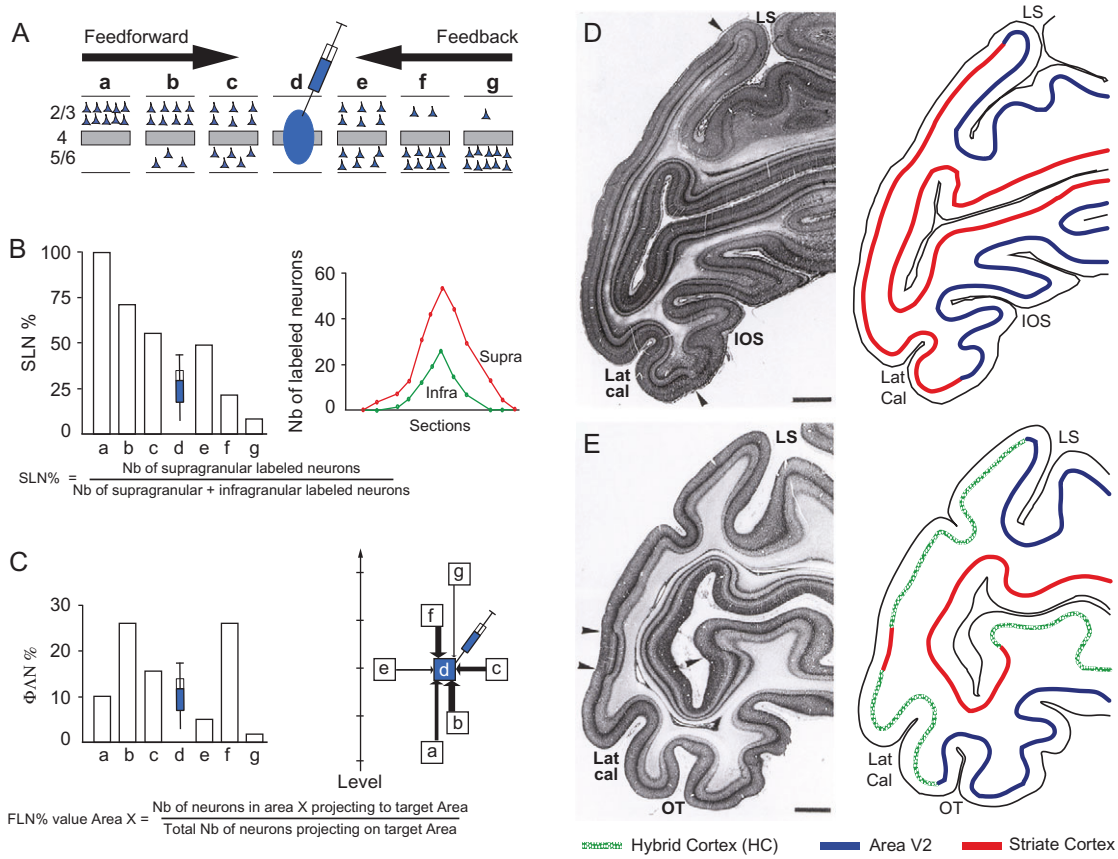

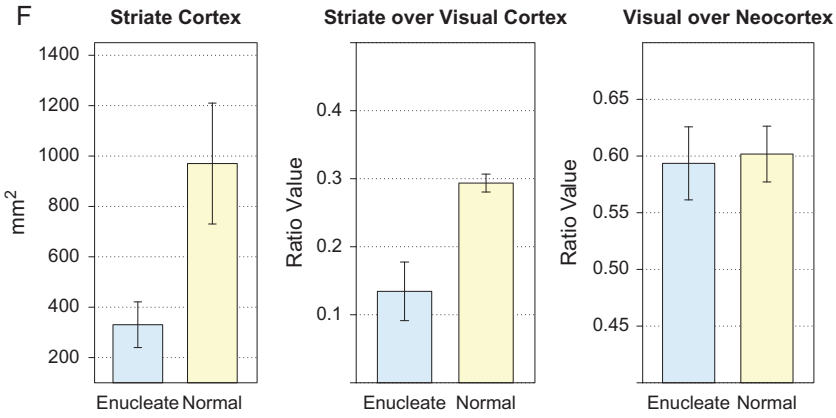

Figure 2. Quantitative parameters characterizing the hierarchy (*A–C*). (*A*) The laminar distribution of parent neurons in each pathway, referred to as SLN (fraction of supragranular neurons) is determined by high frequency sampling and quantitative analysis of labeling. Supra- and infragranular layer neurons contribute to both feedback and feedforward pathways, and their relative proportion is characteristic for each type of pathway. For a given injection there is a gradient of SLN of the labeled areas, between purely FF (SLN = 100%, all the parent neurons are in the supragranular layers) to purely FB (SLN = 0%, all the parent neurons in the infragranular layers) and a spectrum of intermediate proportions. (*B*) All labeled areas can then be ordered by decreasing SLN values and this order is consistent with hierarchical order according to Felleman and Van Essen. SLN is thus used as an indicator of hierarchical distance between areas from the same injection (Barone et al. 2000; Vezoli et al. 2004); (*C*) FLN (fraction of labeled neurons) indicates the relative strength of each pathway (in number of labeled neurons) compared with the total number of neurons that are labeled in the cortical hemisphere after the injection. It requires counting labeled neurons from sections spanning the whole brain, but gives insight into the weight of connections. Vezoli et al. (Vezoli et al. 2004) showed that short-distance connections have high FLN values, whereas the strength of connection decreases as physical distance between source and target areas increases. Effects of early enucleation on cortical parcellation (*D–F*). (*D*) Left panel parasaggital Nissl stained section in a normal neonate showing cytoarchtecture; right-hand panel schematic showing the limits of striate cortex with visibly thick layer 4 and area V2; (*E*) Left panel, parasaggital Nissl stained section in the neonate following prenatal enucleation at 68 days after conception (E68); right-hand panel, limits of areas V1, V2, and hybrid cortex. Sections in *D* and *E* taken from equivalent levels, arrow heads indicate limits of striate cortex. Note, large reduction of striate cortex on operculum and more modest reduction in the calcarine, scale bars, 2 mm. (*F*) Quantitative effects of enucleation on proportions of visual cortex; left-hand panel, surface area of striate cortex ($t_{11} = 6.57$, $P = << 0.001$, 7 enucleates, 6 normals); middle-panel, proportion of striate cortex with respect to total visual cortex ($z = 8.72$, $P << 0.001$, 7 enucleates, 6 normals); right-hand panel, proportion of visual cortex with respect to total cortex ($z = 0.53$, $P = 0.59$, 6 enucleates, 6 normals); Error bars, SD. (*D*) and (*E*) area reproduced from (Dehay et al. 1996a, 1996b) with permission.

proportions of total visual cortex (including HC) with respect to neocortex, which is similar in anophthalmics and normal control, therefore coherent with deafferentation causing a border shift rather than merely a shrinkage of area V1. Hence the HC plus the remaining area V1 in the anophthalmic matches the extent of area V1 in the normal animal (Dehay et al. 1991).

We used retrograde tracers that allow exploring the intrinsic labeling of a cortical area, which corresponds to the local connectivity (Markov et al. 2011). In the normal brain, intrinsic connectivity represents 80–90% of the total connectivity and exhibits an exponential decline with distance (Markov et al. 2011; Horvat et al. 2016) described by the following equation:

$$R(d) = ke^{-\lambda d},$$

where, R is the relative neural count (number of neurons at distance, d, in mm, divided by the total number of intrinsic neurons), k is a free parameter and λ is a scale factor. $1/\lambda$ is called the space constant. It corresponds to the distance in mm at which the relative density falls to the value $e^{-1} \approx 0.37$ and serves as a conventional measure of the spread of the exponential decline. The parameters are estimated as the values that minimize the squared error between the equation and the data, that is, by a least squares criterion. In the anophthalmic brain the space constant of the exponential decline is significantly larger and intrinsic projections extend over considerable distances (Fig. 3A). A convenient measure of comparison is the distance over which a fixed-percentage of the intrinsic labeled neurons is found, the X% threshold, where X% is the percentage of neurons within that distance of the injection site. Hence in the normal V1 the 75% threshold is at 0.85 mm, the 80% at 0.95 mm, and the 95% at 1.7 mm. In the HC, these distances are increased 4 to 6-fold (Fig. 3B), so that local connectivity extends across a large extent of the HC on the operculum (Fig. 4).

Effects of Enucleation on Inputs to HC and Area V2 From Dorsal and Ventral Streams

The HC was injected in 2 anophthalmics and in both cases there were 2 major changes in connectivity. Firstly, there was an increase in the weight of inputs from the ventral stream. Secondly, HC received a strong input from striate cortex that was particular in stemming uniquely from the supragranular layers.

High frequency sampling of labeled neurons in the cortex allows characterization with a single injection of the weighted connectivity of a pathway linking any 2 cortical areas (Markov, Ercsey-Ravasz, et al. 2014). Injections limited to the grey matter were performed in HC, V2, and V4 in 3 anophtalmic brains (Fig. 1 and Table S1). Inspection of cortical labeling suggested that early visual deafferentation leads to an increase of numbers of labeled neurons in ventral stream areas projecting to HC and area V2 (Fig. 4 and Fig. S1). We use counts of labeled neurons to quantify weights of connections (Fig. 2A). Both cases in which injections were made in HC and the injection in area V2 show that deafferentation profoundly affects the relative strengths of the dorsal and ventral pathways, as seen after summing the FLN values across all ventral versus dorsal stream areas (Figs 3C,D and 5, Fig. S2). Differences between normal and anophthalmic cumulative FLN values were not found to be significant following injections in area V4, suggesting that the effects of deafferentation are restricted to early cortical areas.

In summary, these quantifications of the results show that the increase in the proportion of ventral stream projections shown in Figure 2C is not the consequence of a massive change in the weight of a restricted group of areas but is rather spread out across the full complement of ventral stream areas as shown in Figures 5 and S2.

In addition to the increase in the ventral stream, in 1 of the 2 cases of HC injection we found weak labeling in the entorhinal and subiculum cortices. These projections were unexpected as none of the early extrastriate cortical areas in macaque receive projections from either of these cortical areas, although there is a weak projection from entorhinal cortex TEpd (Markov, Ercsey-Ravasz, et al. 2014). In the case that did not reveal projections from subiculum and entorhinal cortex, the injection was extremely small and entirely restricted to the supragranular layer (Fig. S1), which could be the cause of the negative finding in this animal.

The laminar distribution of retrogradely labeled parent neurons of a pathway is defined by its proportion of SLN or SLN index, which has been shown to be highly consistent across individuals (Markov, Vezoli, et al. 2014). The SLN values of a pathway define it as feedforward or feedback and specify a hierarchical distance (Barone et al. 2000). In the absence of the retina there is an increase in numbers of labeled SLN (Fig. 6). Significance is indicated by the differences in logit values for each comparison indicated in the lower panel in A–C in Figure 6. Note, differences between areas are significant when the 95% confidence intervals exclude zero. The SLN value for area V2 projections to HC is significantly higher than for the V2 projection to V1 and likewise the projection of V3, FST and PIP to HC have significantly increased SLN values (Fig. 6A). Following deafferentation, projections to area V2 showed significant increases in the SLN in areas V1 and V3 as well as the dorsal stream areas MT, V3A, LIP, PIP, STP, and PGa as well as an increase in the ventral stream area TEO (Fig. 6B). By contrast, deafferentation had little or no effect on the SLN values for any of the projections to area V4 (Fig. 6C) with the marked exception of V1 where only infragranular neurons were observed. However, given the very low FLN value, this is not considered significant. The most marked change in the SLN is the projection of area V1 to the HC (Fig. 7A). Labeled neurons in area V1 projecting to the HC are entirely located in the supragranular layers, which make this projection very different from any projection from area V1 in the normal brain (Fig. 7B). In the normal area V1 also projects strongly to area V2, but the V1→V2 pathway originates from both infra- and supragranular layers. A projection of V1 which is entirely from the supragranular layers would be to area V4, but the V1→V4 pathway is considerably weaker than the V1→HC pathway (in Fig. 7B, compare the left hand panel with the adjacent panel). Similarly, the second case in which HC was injected also showed a strong projection from the supragranular layers of area V1 to HC (Fig. S1).

In summary, FLN and SLN indices show significant changes for injections in HC and area V2 but not for injections in area V4.

Effects of Enucleation on Cortical Hierarchy

The laminar distribution of neurons gives a measure of hierarchical distance (Barone et al. 2000). This requires charting labeled neurons throughout the projection zones and calculating the SLN (Fig. 2A). Previously we have shown that SLN values extracted from injections at different levels and then mapped onto a hierarchical dimension by means of a sigmoid function display a surprising regularity (Markov, Vezoli, et al. 2014). In brief, we transformed the SLN values by the sigmoidal function

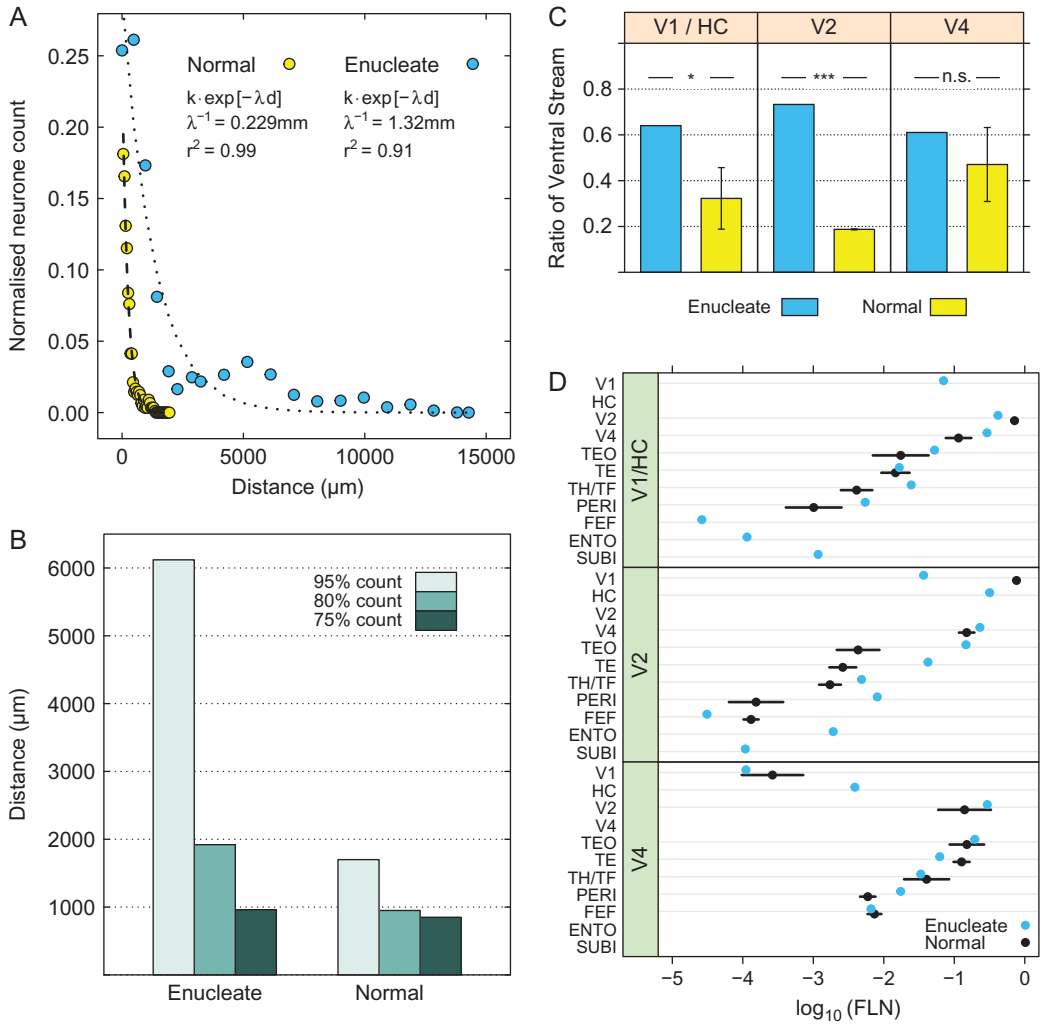

Figure 3. Intrinsic connectivity following enucleation and effects of the weights of input from ventral stream areas (ventralization). (*A*) Exponential decay of density of intrinsic neurons with distance following injection in area V1 of a normal (yellow dots, dashed line fit) and in the HC (enucleation at E73) (blue dots, dotted line fit). The dashed and dotted lines represent exponential fits. (*B*) Distances within which the 3 thresholds (75%, 80%, and 95%) of intrinsic labeling are attained in normal V1 and in the HC (enucleation at E73). (*C*) mean cumulative sum of Fraction of Labeled Neurons (FLN) in ventral stream areas; far-left panel, injections in area V1 and hybrid cortex (HC; $z = -2.42$, $P = 0.016$); middle panel, injections in area V2 ($z = -226.6$, $P << 0.001$); right-hand panel, injections in area V4 ($z = -1.04$, $P = 0.301$). Enucleate versus normal across all injection: ($z = -3.66$, $P = 0.0003$) error bars, SD. All tests were performed assuming that the proportions followed a beta distribution (Cribari-Neto and Zeileis 2010). (*D*) Effect of enucleation on connexion strength in ventral stream areas. Log scale dot plot of FLN. Enucleates, blue dots; normal controls, black dots; upper-panel, injections in normal striate cortex (V1) and hybrid cortex (HC) (1 enucleate, 5 normals); middle-panel, injections in area V2 (1 enucleate, 3 normals); bottom panel, injections in area V4 (2 enucleates, 3 normal); error bars, SD. For abbreviations of area names see glossary.

given by the inverse of a cumulative Gaussian function (or probit function). When these values for the common projections to different injection sites are plotted in a pairwise fashion, the points cluster around lines of slope = 1 (Fig. 7C,D). The implications of this follow from the following reasoning. Suppose that SLN is related to the hierarchical distance between an injected area *A* and an area projecting to it *C*, through some function, *d*, of the SLN that maps SLN values to this distance, so that $d(\mathrm{SLN}_{C\to A}) = d_{CA}$ corresponds to the hierarchical distance between *A* and *C*, indicated by the arrow d_{CA} in Figure 7E. If this distance measure does not depend on the area injected nor the pairs of areas compared, then for injections in areas *A* and *B* that have a common projection *C*, the distance $d_{CA} = d_{CB} + d_{AB}$ (where, the distance between area *C* and *B* is indicated by the arrow d_{CB}). Given that this relation does not depend on the particular common area *C*, it will be true for the entire common projections to areas *A* and *B*, which all differ by the fixed distance between areas *A* and *B*. This is illustrated by considering a different common projection to areas *A* and *B* from an area *D*, indicated by the arrows d_{DA} and d_{DB}, respectively. Again, the distance to both common areas differs by the distance between the 2 injected areas *A* and *B* (indicated by the arrow d_{AB}). The appropriately transformed SLN values from common areas to 2 injection sites when plotted against each other will cluster along a line of unit slope (e.g., the blue dashed lines in Fig. 7C,D). Here, following transformation of the axes by a probit function, the intercept of the line indicates the distance between the 2 injection sites, d_{AB}. We chose the sigmoidal probit function because such functions are often found to map variables defined on the interval (0, 1) to a linear scale (a logit transformation defined as $\log_e(SLN/(1 - SLN))$, would work just as well). Importantly, both the normal and anophthalmic brains display this consistency in laminar organization (Fig. 7C,D). All of the common projections to areas V1 and V2 in

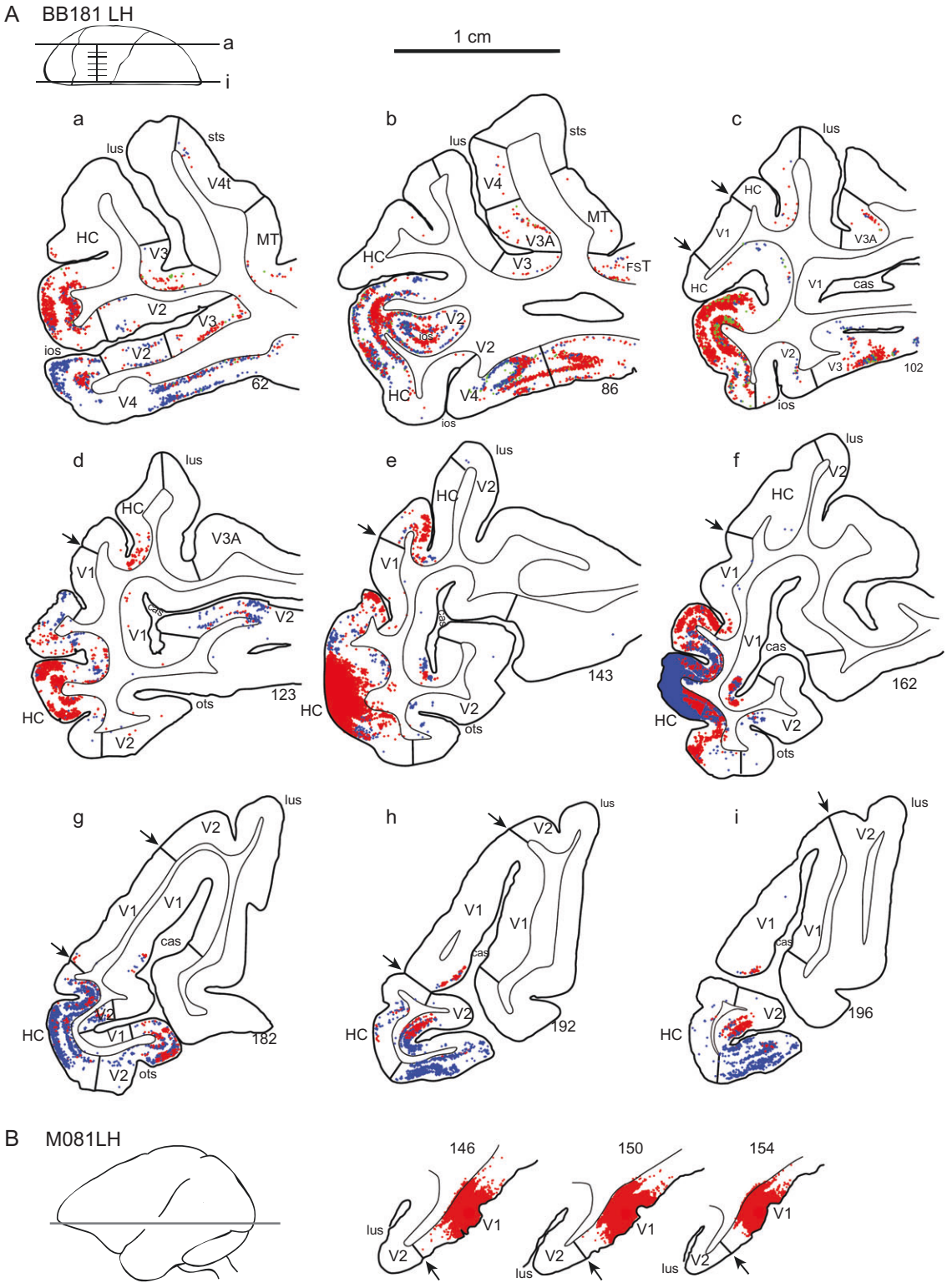

Figure 4. Effect of enucleation on topology of cortical projections to hybrid cortex (HC); parafoveal representation. (*A*) Charts of labeled neurons in low magnification parasagittal sections following paired side-by-side injections in the HC following enucleation at E73. (*B*) Intrinsic labeling in area V1 of a normal macaque brain. Abbreviations: red dots diamidino-yellow-labeled neurons; blue dots, fast blue neurons; arrow heads, V1 borders.

the normal cortex are feedback and, as expected, are observed in the lower left quadrant. This contrasts with the anophthalmic where V1 is in the top right quadrant, indicating it to be feedforward to both HC and V2.

While the above approach could be used to estimate the relative hierarchical distances between pairs of injected areas, we have previously proposed a more global model that includes hierarchical distance estimates between all common projections

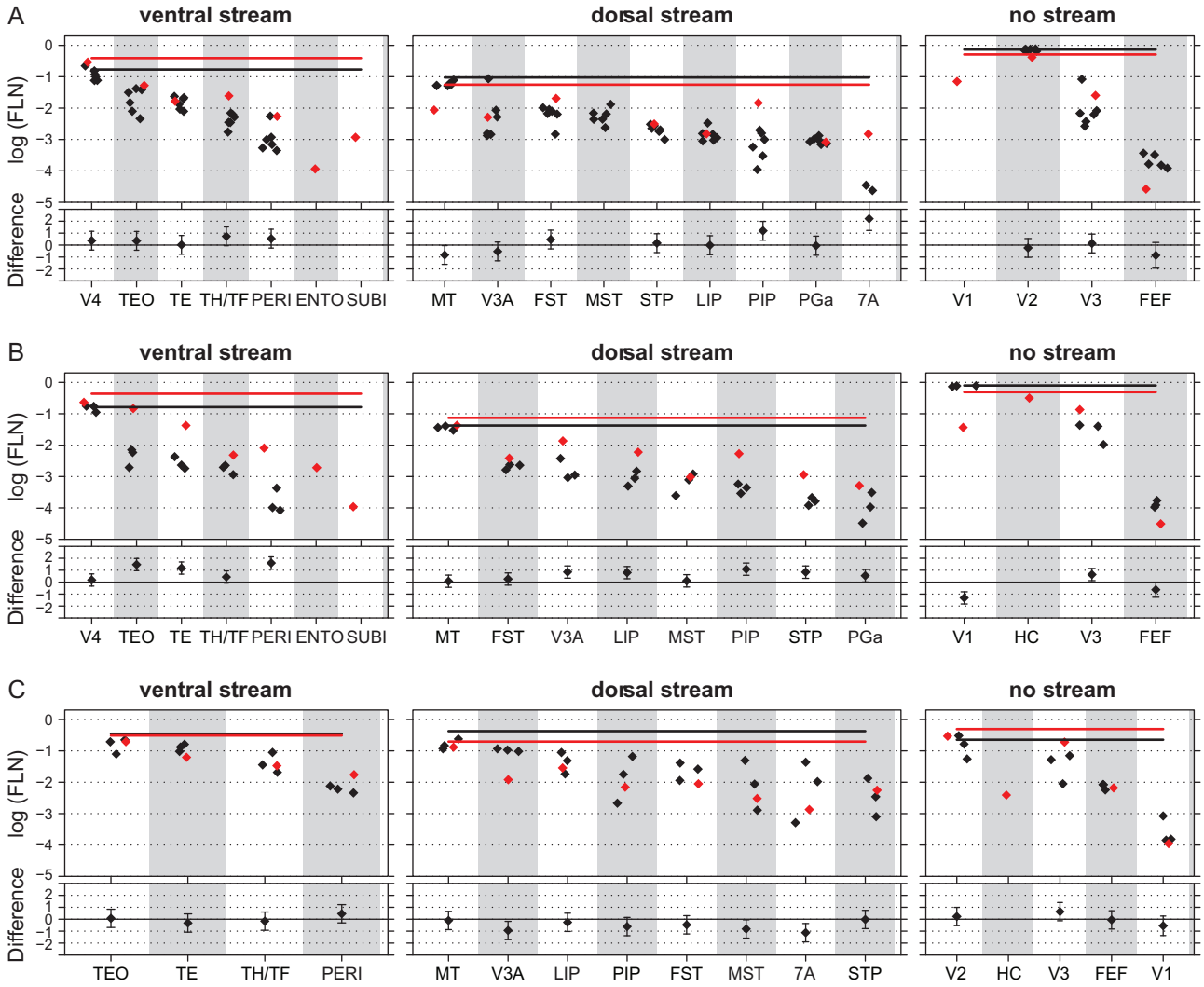

Figure 5. Effects of enucleation on a widespread increase in FLN values to projections to HC and area V2 but not to area V4. Enucleates, red diamonds; normal controls, black diamonds. Mean cumulative sum of functional stream areas, enucleate red line; normal, black line. Upper part, log scale barchart of the fraction of labeled neurons (FLN); lower part, estimated difference and 95% confidence interval (intervals that do not include zero indicate significant differences). (A) Injections in normal striate cortex representing the central area V1 and equivalent regions in hybrid cortex (BB181 HC; 1 enucleate, 6 normals). (B) Injections in area V2 (1 enucleate, 3 normals). (C) Injections in area V4 (3 enucleate, 1 normal). For abbreviations of area names see glossary.

to the injection sites (Markov, Vezoli, et al. 2014). We assume that the SLN values are related to a latent linear model that estimates values representing the hierarchical distance between pairs of areas through a nonlinear link function, g. The model is formalized by the following equation:

$$g(\mathrm{E}(\mathrm{SLN})) = X\beta,$$

where, the link function g, transforms the expected value of SLN, which is related to the product of a matrix, X and a vector β. X is a $n \times p$ incidence matrix for the cortical connectivity graph, with a column for each of p areas and a row for each of n pairs of connected areas (repeated injections may appear as multiple rows). All elements of X are 0 except in the 2 columns corresponding to the connecting pairs for that row, taking on the values −1 and 1 for the target and source, respectively. Since, by construction, each row adds to 0, one column is dropped for model identifiability, fixing the coefficient corresponding to that column at 0. β is a vector of hierarchical values to be estimated with one value omitted, corresponding to the dropped column. The action of the matrix X on the vector β is to extract the difference in hierarchical values, $\beta_j - \beta_i$ for the row corresponding to the projection from area j to i. A probit (inverse cumulative Gaussian) function is used for the link function g, though equivalent results are obtained by using a logit of the SLN (natural log of the ratio of supragranular and infragranular neurons) since when properly scaled both functions are nearly identical over the range of interest. The model resembles a GLM with a binomial family (McCullagh and Nelder 1989), but the data are over-dispersed so a model that includes a dispersion estimate is used instead. The hierarchical levels are estimated by maximum likelihood assuming that the SLN values follow a beta-binomial distribution (Lesnoff and Lancelot 2012; R Development Core Team 2016). Further details can be found in Markov, Vezoli, et al. (2014).

Considering the ensemble of SLN values following injections in areas V1, V2, and V4, we fit the above hierarchical model to both the normal and anophthalmic data sets (Fig. 8A) (Markov, Vezoli, et al. 2014). The estimated hierarchical coefficients are only determined up to a linear transformation so that the

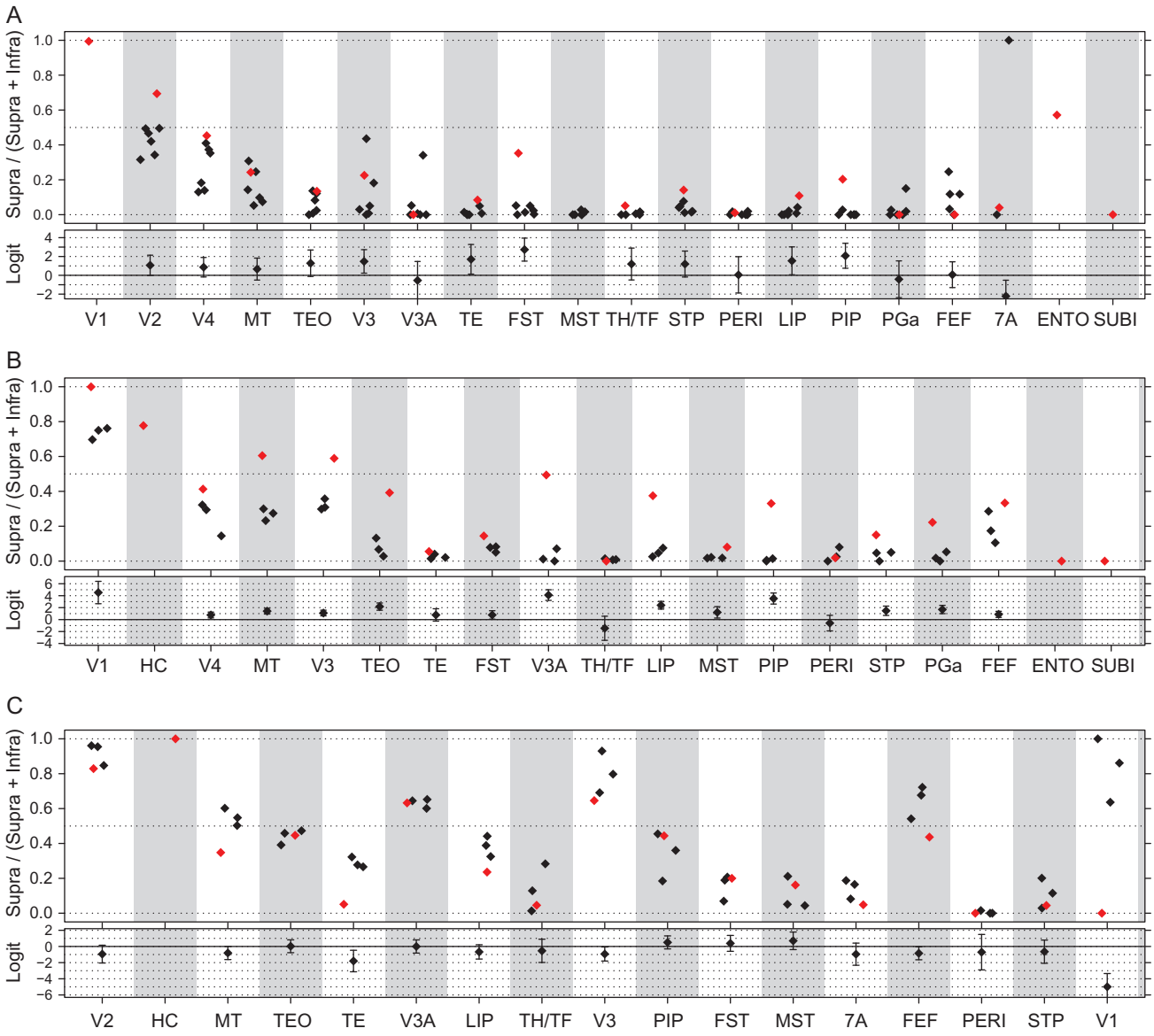

Figure 6. Effects of enucleation on SLN. Enucleates, red diamonds; normal controls, black diamonds. Upper part: ratio of numbers of labeled supragranular layer neurons divided by the sum of labeled supra- and infragranular neurons. Lower part, estimated difference and 95% confidence interval (intervals that do not include zero indicate significant differences). (*A*) Injections in normal striate cortex representing the central area V1 and equivalent regions in Hybrid Cortex (HC; 1 enucleate, 6 normals). (*B*) Injections in area V2 (1 enucleate, 3 normals). (*C*) Injections in area V4 (3 enucleate, 1 normal). For abbreviations of area names see glossary.

values in the figures have been scaled to the range 1–10. The results show that the overall layout of the ventral and dorsal stream areas remains approximately similar to that observed in the normal. However, in the anophthalmic brain, HC and area V2 are considerably higher in the hierarchy than expected.

To evaluate the goodness of fit of the model, the empirical values of SLN were compared with those predicted by the model. The comparison of these are shown in Figure 8*B*. The predicted values were obtained by substituting the estimated coefficients in the model of the linear predictor and applying the inverse link function (a cumulative Gaussian function). Standard errors were calculated for the SLN predictions by using the variance–covariance matrix to estimate standard errors on the scale of the linear predictor and transforming these back to the SLN scale by the inverse link function (see Markov, Vezoli, et al. 2014 for further details).

The goodness of fit of the model is shown by the comparisons between the empirical and model estimated SLN values plotted by source and target areas (Fig. 8*B*, normal $r^2 = 0.72$; enucleate $r^2 = 0.67$). The close overall agreement in predicted and empirical SLN values supports that the model and the hierarchical values estimated from it provide an accurate summary of the laminar relations among areas and their gradient across the cortex.

Discussion

Comparison the Developmental Effects in Macaque of Eye Removal on Other Animal Models of Congenital Blindness

The present findings contrast with those obtained in a recent study on the effects of bilateral enucleation in *Mondelphis*

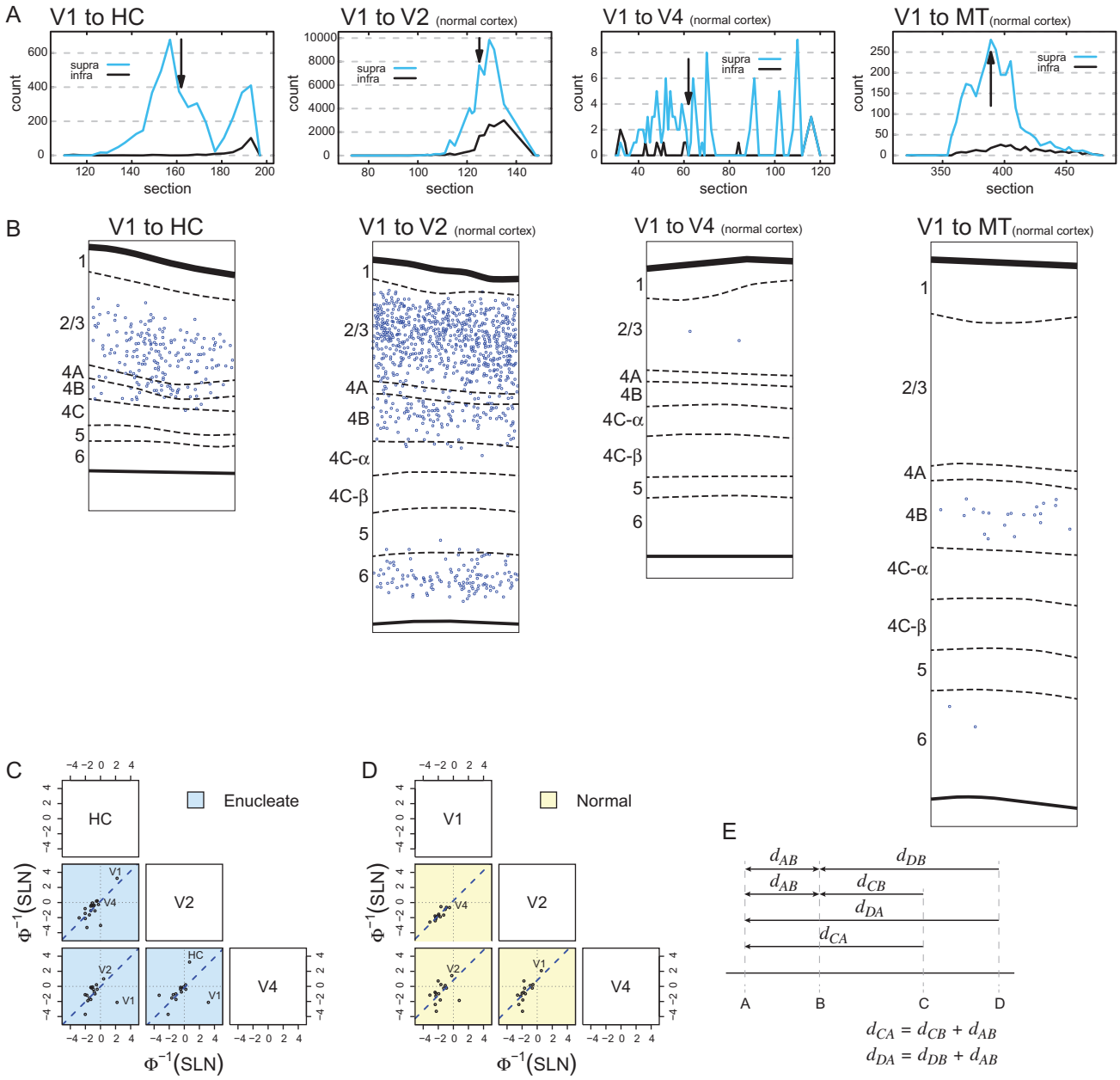

Figure 7. Laminar distribution of labeled cells and hierarchy. (*A*) Density profiles showing changing proportions of labeled supra- and infragranular neurons in individual sections at different point in the projection zones following injections in HC (far-left panel), V2, V4, and V1 (far-right panel). Black arrows in the connectivity profiles indicate the section used for high power plots. (*B*) High power plots comparing laminar distributions of V1 → HC to projections in the normal cortex. Individual plots taken from locations returning peak levels of labeled neurons indicated by back arrows in the connectivity profiles shown in "A." This comparison shows that the V1 → HC has no counterpart in the normal cortex, either in terms of strength of projection nor laminar distribution. (*C*) and (*B*) Pairs plots between probit-transformed SLN values of common areas from injections in V1/HC, V2, and V4 (as indicated in the boxes along the diagonal). Each point represents the average pair of SLN values obtained in a single source area; the blue dashed lines indicate the best fitting lines of unit slope. (*C*) Enucleated cases (blue background). (*D*) Data from normal controls (yellow background). Area labels for points of potential interest and outliers are indicated to the right of the point. (*E*) Schematic of hierarchical distance relations motivating the pairs plots of SLN values, dxy is the distance between X and Y.

domestica, a South American marsupial (Kahn and Krubitzer 2002; Karlen et al. 2006). These authors found that enucleation at postnatal day 4 led to extensive cortical regions that are normally involved in visual processing being implicated by auditory and somatosensory information processing; electrophysiological findings of cross-modal cortical plasticity were accompanied by abnormal corticocortical and thalamocortical connections. These aberrant projections from nonvisual subcortical structures were accompanied by projections from auditory, somatosensory and multimodal cortical regions. The greater plasticity observed by Krubitzer's group in the marsupial brain compared with the present findings could be due to the differences in development when the retina was removed. There are 2 arguments against this hypothesis. Firstly, while the enucleation at fourth postnatal day in the opossum is at an earlier developmental stage than the enucleation in the macaque at embryonic (E) day 70 (Workman et al. 2013), in both species thalamic innervation of the visual cortex is incomplete and generation of supragranular

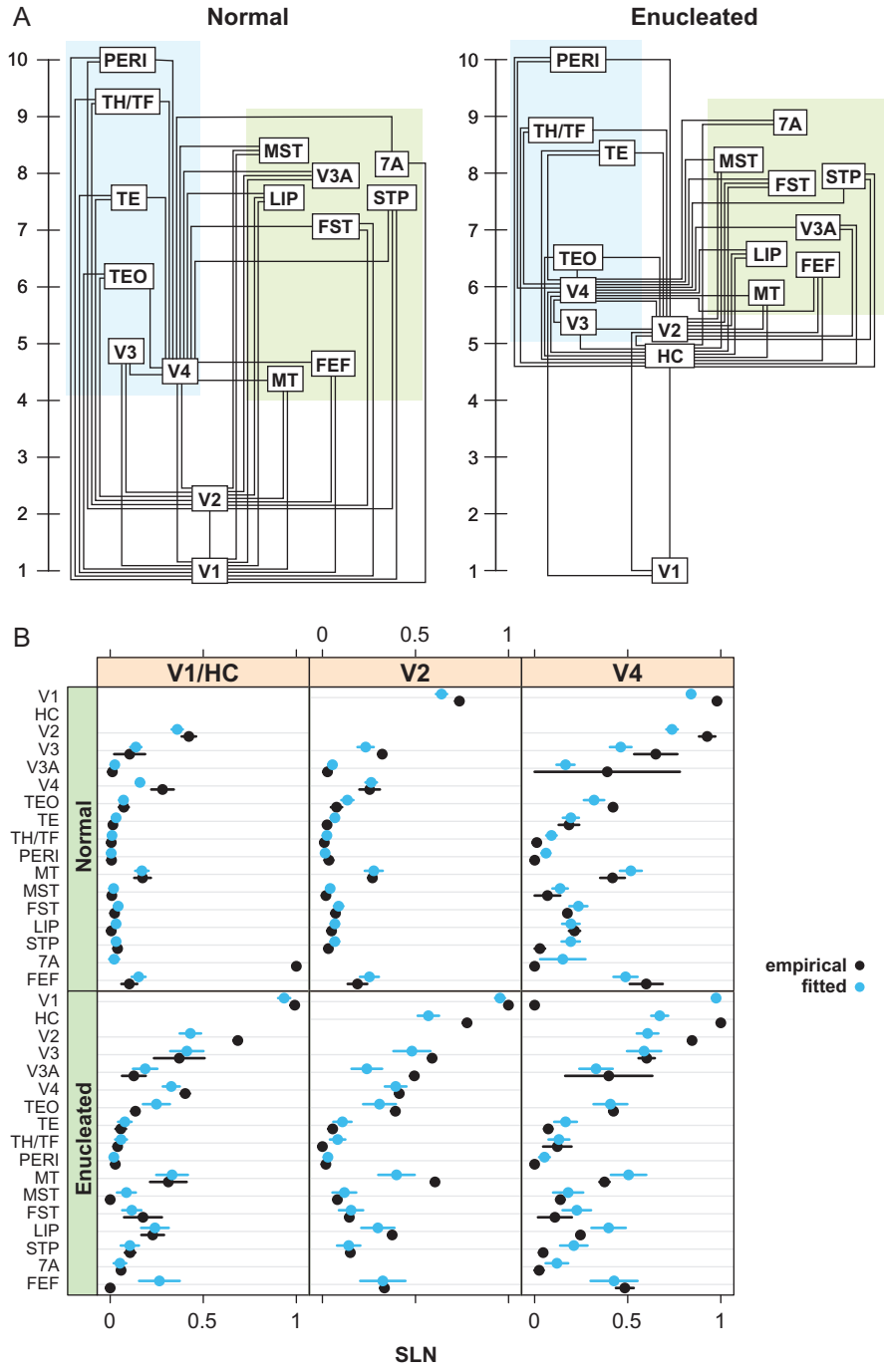

Figure 8. Developmental plasticity of the visual hierarchy. (*A*) Hierarchical relationship between areas in the visual system based on injections in V1, V2 and V4 in normal animals, and following enucleation and injections in Hybrid Cortex (HC), V2, and V4. (*B*) Detailed comparison of the model with the data for each injection by labeled area; black dots, empirical values; blue dots, predicted values. Error bars are empirical SEs for the data and model based SEs for the predictions.

layers has not yet commenced (Rakic 1974; Robinson and Dreher 1990; Finlay and Darlington 1995; Molnar et al. 1998). Secondly, in both species the ages when the retinas were removed lead to profound and very similar modifications of the cortex (Rakic 1988; Dehay et al. 1989; Kahn and Krubitzer 2002), with the generation of a novel cortical region referred to as area X by Rakic (1988) and HC in the present study. Hence, it would seem that the observed differences between the results obtained are related to species with different evolutionary histories and perhaps differing developmental susceptibilities that could conceivably be related to differences in brain size (Chalupa and Dreher 1991).

It has frequently been postulated that cortical connections of visual cortex are initially widely distributed and that transient projections from inappropriate areas are eliminated during development, so that the adult pattern of connectivity is viewed as the consequence of a process of selective elimination often referred as developmental pruning of exuberant connections (Innocenti and Price 2005). For instance, in a wide range

of species including carnivores and rodents, callosal connections linking the visual cortices in the 2 hemispheres are initially widespread and become progressively restricted to the representation of the vertical meridian via axon elimination. Removal of the retina early in development has been shown to interfere with the developmental removal of these transient connections (Innocenti and Frost 1979; Rhoades and Dellacroce 1980; Cusick and Lund 1982; Olavarria and Van Sluyters 1984). Transient connections that are selectively eliminated during development are not restricted to pathways linking the 2 hemispheres; in the newborn cat there are projections from the frontoparietal and temporal cortex to areas 17, 18, and 19 (Dehay et al. 1984; Innocenti and Clarke 1984).

Macaque is very different in one major respect, there are no transient callosal connections in area 17 (Dehay et al. 1988), nor are there transient exuberant association projections involving the visual system throughout development (Barone et al. 1995, 1996; Batardiere et al. 2002). These findings could well mean that the more prolonged development of primates is characterized by more restricted instances of exuberant cortical connectivity during development. Hence, in contrast to the findings in opossum (Karlen et al. 2006), in macaque the absence of projections from auditory and somatosensory cortices to early stages of cortical processing following developmental absence of the retina could simply reflect the absence of these pathways during normal primate development.

The critical feature that underlies the profound influence of the retina on cortical development in the primate could be differences in the development of thalamus and cortex in primates and rodents (Kennedy and Dehay 1993a; Dehay and Kennedy 2007). The timing of thalamic development in primates is comparable to what is found in nonprimates, contrasting with corticogenesis, which is relatively prolonged being characterized by very long cell-cycle durations (Kornack and Rakic 1998; Lukaszewicz et al. 2005). This heterochronicity in the timing of development in thalamus and cortex development (Kennedy and Dehay 1993b) means that the bulk of corticogenesis occurs later in primates compared with rodents (Finlay and Darlington 1995). Enucleation in macaque influences corticogeneis maximally when carried out before E80, when fibers from the lateral geniculate nucleus are in close proximity with the outer subventricular zone. The lateral geniculate fibers that can influence the kinetics of the cell-cycle of cortical precursors by release of a mitogenic substance (Dehay et al. 2001; Dehay and Kennedy 2007), which would have a profound influence on the cell lineages of cortical precursors generating upper layers of the cortex (Betizeau et al. 2013).

Hierarchy in the Normal and Anopthalmic Brain

Elsewhere we have shown that in macaque laminar relations as quantified by SLN reveal a surprising degree of regularity in cortical organization (Markov, Vezoli, et al. 2014). Specifically, the SLN values amongst sets of cortical areas match in such a way as to be internally consistent, and this consistency determines a hierarchical order. Elsewhere we have shown that this structural order reflects a functional organization of the macaque cortex (Bastos et al. 2015). Remarkably, the present results show that when a new area is introduced (i.e., HC) accompanied by a new V1→HC projection, the full set of SLN values exhibit appropriate adjustment. This observation is very provocative because it would suggest that there is a corresponding functional reorganization. The fact that the human brain shows the same structural/functional correspondence as described in macaque (Michalareas et al. 2016), suggests that theses areal relationships could be usefully explored in the congenital blind.

Relevance of Developmental Effects of Eye Removal in Macaque on Congenital Blindness in Human

The present results show that in the anophthalmic macaque the topography of connectivity and global organization of the ventral and dorsal streams are largely conserved as has been suggested by imaging studies in the human congenitally blind (Pietrini et al. 2004; Ptito et al. 2009; Matteau et al. 2010; Striem-Amit, Cohen et al. 2012; Striem-Amit, Dakwar, et al. 2012, 2015; van den Hurk et al. 2017), in line with the evidence of early developmental specification of the functional streams (Deen et al. 2017; Livingstone et al. 2017). Further, in the anophthalmic brain we observe an expansion of the ventral pathway that could reflect cross-modal plasticity (Ptito et al. 2009).

The early primate visual cortex in anophthalmia is profoundly modified both in its cytoarchitecture and local connectivity. While the global hierarchy remains largely conserved, there are important local changes in the hierarchical organization. These changes would seem to reflect a persistence of immature features making the congenitally blind "visual" cortex neotenic. Indeed, interareal connectivity during in utero development in the primate undergoes extensive remodeling characterized by a greatly expanded population of supragranular projecting neurons, a global hierarchical organization similar to that found in the adult, an absence of ectopic pathways and finally a markedly extensive local connectivity (Luhmann et al. 1986; Barone et al. 1995; Khazipov and Luhmann 2006; Markov, Vezoli, et al. 2014). The relatively high position in the cortical hierarchy and the conservation of an extensive local connectivity in the HC could ensure the long-time constants with neuronal response over seconds, which would be required for the observed higher cognitive functions of the deafferented cortex of the blind (Honey et al. 2012; Chaudhuri et al. 2015).

The present results provide evidence of an induced projection of the subiculum and entorhinal cortices on to HC. One can speculate that this pathway could contribute to the functional reorganization of the cortex and may lead to improved semantic and episodic memory that has been reported in human congenital blindness (Amedi et al. 2003; Pasqualotto et al. 2013).

It is now increasingly recognized that theories of brain organization need to be cast in both functional and structural terms. The high density of the cortical graph combined with the wide range of interareal weights underlines the importance of the spatial embedding of cortical networks as a principal organizational feature (Markov et al. 2013; Roberts et al. 2016). Alignment of structural maps with surface electrode recording has made it possible to define functional hierarchies first in the macaque and subsequently extrapolated to the human brain (Bastos et al. 2015; Michalareas et al. 2016). The structural data in the present study can be exploited in a similar fashion in future electrophysiological recordings in anophthalmic monkeys and congenitally blind human, as well as for exploring how developmental plasticity can influence cortical hierarchical timescales (Hasson et al. 2008, 2016; Chaudhuri et al. 2015; Cocchi et al. 2016).

The present results suggesting that there is an expansion of the connectivity of the occipitotemporal cortex in the congenital blind brain with indications that the entorhinal and subiculum access the HC need to be considered with respect to

present day understanding of the processing of the ventral visual pathway (Kravitz et al. 2013). However, the present study is only a partial study of the visual pathways of the anophthalmic monkey. Given the greater emphasis of the peripheral visual field in the dorsal stream (Ungerleider et al. 2008; Kravitz et al. 2011), one could speculate that the striate cortex in the calcarine of the anophthalmic monkey might show a very different connectivity to that of the HC that we have explored in the present study, which would correspond to a foveal area V1.

Conclusion

The present findings need to be considered in view of current understanding of the developmental specification of the cortex. Developmental patterning of the neocortex is consequent to an interplay between intrinsic genetic mechanisms based on morphogens and secreted signaling molecules and extrinsic inputs relayed to the cortex by thalamocortical axons (O'Leary et al. 2007; De la Rossa et al. 2013; Geschwind and Rakic 2013). The role of thalamic axons in arealization is a multistep hierarchical process involving events at progenitor and neuronal levels (Chou et al. 2013; Pouchelon and Jabaudon 2014; Moreno-Juan et al. 2017). The present findings confirm Rakic's suggestion that depletion of thalamic axons reveals the interplay between intrinsic and extrinsic factors controlling arealization and that this will lead to a HC combining features that are found in different areas in what constitutes a de novo area. However, in rodent genetic depletion of the thalamic input to the primary visual area shows that intrinsic mechanisms specify a relatively uniform genetic profile across the occipital cortex suggesting that the thalamic input is necessary for the patterned gene expression that distinguishes primary and higher order areas (Chou et al. 2013). By contrast the areal dimensions and connectivity were not altered following depletion of thalamic afferents to the cortex. This contrasts with the present study where we show that the HC exhibits a unique connectivity profile combining the spatially extended local connectivity of frontal areas and a unique hierarchical relation to other visual areas. These differences in primate and rodent on the role of thalamic afferents to the cortex could reflect the early and prolonged thalamic innervation of the germinal zones in the primate compared with the rodent.

A recent spatiotemporal transcriptome analysis of the prenatal and postnatal macaque forebrain revealed a small number of genes that have persistent expression across cortical development, suggesting a large potential for extrinsic shaping of the cortex (Bakken et al. 2016). Interestingly, this study shows that areal and laminar molecular phenotypes are acquired late postnatally indicating a wide and potentially important role of contextual shaping of the structure and function of the cortex. These observations, inline with the profound effects of afferent specification of cortex in the present study suggest that particular attention should be paid to the education and the special needs and perhaps capacities of the young congenitally blind with respect to the dorsal (Cappagli et al. 2017) but also the ventral pathway.

Supplementary Material

Supplementary material is available at *Cerebral Cortex* online.

Funding

LABEX CORTEX (ANR-11-LABX-0042) of Université de Lyon (ANR-11-IDEX-0007) operated by the French National Research Agency (ANR) (H.K.), ANR-11-BSV4-501, CORE-NETS (H.K.), ANR-14-CE13-0033, ARCHI-CORE (H.K.), ANR-15-CE32-0016, CORNET (H.K.), ANR-17-NEUC-0004, A2P2MC (H.K.), ANR-17-HBPR-0003, CORTICITY (H.K.).

Author contribution

C.D., H.K. proposed the research; P.G., M.B., H.K. surgical intervention; P.B., P.G., C.D. histological processing; L.M., P.B., N.T.M., P.G., H.P.K., data acquisition; L.M., P.B., N.T.M., K.K., H.K. data analysis; K.K. computational modeling; L.M., K.K., C.D., H.K. wrote the article. All authors contributed to editing the final document.

Notes

Conflict of Interest: None declared.

References

Alfano C, Magrinelli E, Harb K, Hevner RF, Studer M. 2014. Postmitotic control of sensory area specification during neocortical development. Nat Commun. 5:5632.

Amedi A, Floel A, Knecht S, Zohary E, Cohen LG. 2004. Transcranial magnetic stimulation of the occipital pole interferes with verbal processing in blind subjects. Nat Neurosci. 7:1266–1270.

Amedi A, Raz N, Pianka P, Malach R, Zohary E. 2003. Early 'visual' cortex activation correlates with superior verbal memory performance in the blind. Nat Neurosci. 6:758–766.

Bakken TE, Miller JA, Ding SL, Sunkin SM, Smith KA, Ng L, Szafer A, Dalley RA, Royall JJ, Lemon T, et al. 2016. A comprehensive transcriptional map of primate brain development. Nature. 535:367–375.

Barone P, Batardiere A, Knoblauch K, Kennedy H. 2000. Laminar distribution of neurons in extrastriate areas projecting to visual areas V1 and V4 correlates with the hierarchical rank and indicates the operation of a distance rule. J Neurosci. 20:3263–3281.

Barone P, Dehay C, Berland M, Bullier J, Kennedy H. 1995. Developmental remodeling of primate visual cortical pathways. Cereb Cortex. 5:22–38.

Barone P, Dehay C, Berland M, Kennedy H. 1996. Role of directed growth and target selection in the formation of cortical pathways: prenatal development of the projection of area V2 to area V4 in the monkey. J Comp Neurol. 374:1–20.

Bastos AM, Vezoli J, Bosman CA, Schoffelen JM, Oostenveld R, Dowdall JR, De Weerd P, Kennedy H, Fries P. 2015. Visual areas exert feedforward and feedback influences through distinct frequency channels. Neuron. 85:390–401.

Batardiere A, Barone P, Knoblauch K, Giroud P, Berland M, Dumas AM, Kennedy H. 2002. Early specification of the hierarchical organization of visual cortical areas in the macaque monkey. Cereb Cortex. 12:453–465.

Bavelier D, Dye MW, Hauser PC. 2006. Do deaf individuals see better? Trends Cogn Sci. 10:512–518.

Bavelier D, Neville HJ. 2002. Cross-modal plasticity: where and how? Nat Rev Neurosci. 3:443–452.

Bedny M. 2017. Evidence from blindness for a cognitively pluripotent cortex. Trends Cogn Sci. 21:637–648.

Bedny M, Pascual-Leone A, Dodell-Feder D, Fedorenko E, Saxe R. 2011. Language processing in the occipital cortex of congenitally blind adults. Proc Natl Acad Sci USA. 108: 4429–4434.

Betizeau M, Cortay V, Patti D, Pfister S, Gautier E, Bellemin-Menard A, Afanassieff M, Huissoud C, Douglas RJ, Kennedy H, et al. 2013. Precursor diversity and complexity of lineage relationships in the outer subventricular zone (OSVZ) of the primate. Neuron. 80:442–457.

Buchel C, Price C, Frackowiak RS, Friston K. 1998. Different activation patterns in the visual cortex of late and congenitally blind subjects. Brain. 121:409–419.

Burton H, Sinclair RJ, Agato A. 2012. Recognition memory for Braille or spoken words: an fMRI study in early blind. Brain Res. 1438:22–34.

Cappagli G, Finocchietti S, Baud-Bovy G, Cocchi E, Gori M. 2017. Multisensory rehabilitation training improves spatial perception in totally but not partially visually deprived children. Front Integr Neurosci. 11:29.

Chalupa LM, Dreher B. 1991. High precision systems require high precision "blueprints": a new view regarding the formation of connections in the mammalian visual system. J Cogn Neurosci. 3:209–219.

Chaudhuri R, Knoblauch K, Gariel MA, Kennedy H, Wang XJ. 2015. A large-scale circuit mechanism for hierarchical dynamical processing in the primate cortex. Neuron. 88: 419–431.

Chou SJ, Babot Z, Leingartner A, Studer M, Nakagawa Y, O'Leary DD. 2013. Geniculocortical input drives genetic distinctions between primary and higher-order visual areas. Science. 340:1239–1242.

Cocchi L, Sale MV, L Gollo L, Bell PT, Nguyen VT, Zalesky A, Breakspear M, Mattingley JB. 2016. A hierarchy of timescales explains distinct effects of local inhibition of primary visual cortex and frontal eye fields. Elife. 5:e15252, DOI:10.7554/eLife.15252.

Cohen LG, Celnik P, Pascual-Leone A, Corwell B, Falz L, Dambrosia J, Honda M, Sadato N, Gerloff C, Catala MD, et al. 1997. Functional relevance of cross-modal plasticity in blind humans. Nature. 389:180–183.

Cremisi F, Philpott A, Ohnuma S. 2003. Cell cycle and cell fate interactions in neural development. Curr Opin Neurobiol. 13:26–33.

Cribari-Neto F, Zeileis A. 2010. Beta regression in R. J Stat Soft. 34:1–24.

Cusick CG, Lund RD. 1982. Modification of visual callosal projections in rats. J Comp Neurol. 212:385–398.

De la Rossa A, Bellone C, Golding B, Vitali I, Moss J, Toni N, Luscher C, Jabaudon D. 2013. In vivo reprogramming of circuit connectivity in postmitotic neocortical neurons. Nat Neurosci. 16:193–200.

Deen B, Richardson H, Dilks DD, Takahashi A, Keil B, Wald LL, Kanwisher N, Saxe R. 2017. Organization of high-level visual cortex in human infants. Nat Commun. 8:13995.

Dehay C, Bullier J, Kennedy H. 1984. Transient projections from the fronto-parietal and temporal cortex to areas 17, 18 and 19 in the kitten. Exp Brain Res. 57:208–212.

Dehay C, Giroud P, Berland M, Killackey H, Kennedy H. 1996a. Contribution of thalamic input to the specification of cytoarchitectonic cortical fields in the primate: effects of bilateral enucleation in the fetal monkey on the boundaries, dimensions, and gyrification of striate and extrastriate cortex. J Comp Neurol. 367:70–89.

Dehay C, Giroud P, Berland M, Killackey HP, Kennedy H. 1996b. Phenotypic characterisation of respecified visual cortex subsequent to prenatal enucleation in the monkey: development of acetylcholinesterase and cytochrome oxidase patterns. J Comp Neurol. 376:386–402.

Dehay C, Giroud P, Berland M, Smart I, Kennedy H. 1993. Modulation of the cell cycle contributes to the parcellation of the primate visual cortex. Nature. 366:464–466.

Dehay C, Horsburgh G, Berland M, Killackey H, Kennedy H. 1989. Maturation and connectivity of the visual cortex in monkey is altered by prenatal removal of retinal input. Nature. 337:265–267.

Dehay C, Horsburgh G, Berland M, Killackey H, Kennedy H. 1991. The effects of bilateral enucleation in the primate fetus on the parcellation of visual cortex. Dev Brain Res. 62:137–141.

Dehay C, Kennedy H. 2007. Cell-cycle control and cortical development. Nat Rev Neurosci. 8:438–450.

Dehay C, Kennedy H, Bullier J, Berland M. 1988. Absence of interhemispheric connections of area 17 during development in the monkey. Nature. 331:348–350.

Dehay C, Savatier P, Cortay V, Kennedy H. 2001. Cell-cycle kinetics of neocortical precursors are influenced by embryonic thalamic axons. J Neurosci. 21:201–214.

Donahue CJ, Sotiropoulos S, Jbabdi S, Herandez-Ferandez M, Behrens T, Kennedy H, Knoblauch K, Coalson T, Glasser M, Van Essen D. 2016. Using diffusion tractography to predict cortical connection strength and distance: a quantitative comparison with tracers in the monkey. J Neurosci. 36: 6758–6770.

Eagleson KL, Lillien L, Chan AV, Levitt P. 1997. Mechanisms specifying area fate in cortex include cell-cycle-dependent decisions and the capacity of progenitors to express phenotype memory. Development. 124:1623–1630.

Ercsey-Ravasz M, Markov NT, Lamy C, Van Essen DC, Knoblauch K, Toroczkai Z, Kennedy H. 2013. A predictive network model of cerebral cortical connectivity based on a distance rule. Neuron. 80:184–197.

Finlay BL, Darlington RB. 1995. Linked regularities in the development and evolution of mammalian brains. Science. 268: 1578–1584.

Gattass R, Gross CG, Sandell JH. 1981. Visual topography of V2 in the macaque. J Comp Neurol. 201:519–539.

Gattass R, Sousa AP, Rosa MG. 1987. Visual topography of V1 in the Cebus monkey. J Comp Neurol. 259:529–548.

Geschwind DH, Rakic P. 2013. Cortical evolution: judge the brain by its cover. Neuron. 80:633–647.

Hasson U, Andric M, Atilgan H, Collignon O. 2016. Congenital blindness is associated with large-scale reorganization of anatomical networks. Neuroimage. 128:362–372.

Hasson U, Yang E, Vallines I, Heeger DJ, Rubin N. 2008. A hierarchy of temporal receptive windows in human cortex. J Neurosci. 28:2539–2550.

Honey CJ, Thesen T, Donner TH, Silbert LJ, Carlson CE, Devinsky O, Doyle WK, Rubin N, Heeger DJ, Hasson U. 2012. Slow cortical dynamics and the accumulation of information over long timescales. Neuron. 76:423–434.

Horvat S, Gamanut R, Ercsey-Ravasz M, Magrou L, Gamanut B, Van Essen DC, Burkhalter A, Knoblauch K, Toroczkai Z, Kennedy H. 2016. Spatial embedding and wiring cost constrain the functional layout of the cortical network of rodents and primates. PLoS Biol. 14:e1002512.

Innocenti GM, Clarke S. 1984. Bilateral transitory projection to visual areas from auditory cortex in kittens. Dev Brain Res. 14:143–148.

Innocenti GM, Frost DO. 1979. Effects of visual experience on the maturation of the efferent system to the corpus callosum. Nature. 280:231–233.

Innocenti GM, Price DJ. 2005. Exuberance in the development of cortical networks. Nat Rev Neurosci. 6:955–965.

Kahn DM, Krubitzer L. 2002. Massive cross-modal cortical plasticity and the emergence of a new cortical area in developmentally blind mammals. Proc Natl Acad Sci USA. 99: 11429–11434.

Kanjlia S, Lane C, Feigenson L, Bedny M. 2016. Absence of visual experience modifies the neural basis of numerical thinking. Proc Natl Acad Sci USA. 113:11172–11177.

Karlen SJ, Kahn DM, Krubitzer L. 2006. Early blindness results in abnormal corticocortical and thalamocortical connections. Neuroscience. 142:843–858.

Keizer K, Kuypers HGJM, Huisman AM, Dann O. 1983. Diamidino Yellow dihydrochloride (DY 2HCl): a new fluorescent retrograde neuronal tracer, which migrates only very slowly out of the cell. Exp Brain Res. 51:179–191.

Kennedy H, Dehay C. 1993a. Cortical specification of mice and men. Cereb Cortex. 3:27–35.

Kennedy H, Dehay C. 1993b. The importance of developmental timing in cortical specification. Persp Dev Neurobiol. 1: 93–99.

Khazipov R, Luhmann HJ. 2006. Early patterns of electrical activity in the developing cerebral cortex of humans and rodents. Trends Neurosci. 29:414–418.

Killackey HP. 1990. Neocortical expansion: an attempt towards relating phylogeny and ontogeny. J Cogn Neurosci. 2:1–17.

Kollros JJ, Thiesse ML. 1988. Control of tectal cell number during larval development in Rana pipiens. J Comp Neurol. 278: 430–445.

Kornack DR, Rakic P. 1998. Changes in cell-cycle kinetics during the development and evolution of primate neocortex. Proc Natl Acad Sci USA. 95:1242–1246.

Kravitz DJ, Saleem KS, Baker CI, Mishkin M. 2011. A new neural framework for visuospatial processing. Nat Rev Neurosci. 12:217–230.

Kravitz DJ, Saleem KS, Baker CI, Ungerleider LG, Mishkin M. 2013. The ventral visual pathway: an expanded neural framework for the processing of object quality. Trends Cogn Sci. 17:26–49.

Krubitzer LA, Seelke AM. 2012. Cortical evolution in mammals: the bane and beauty of phenotypic variability. Proc Natl Acad Sci USA. 109(Suppl 1):10647–10654.

Lesnoff M, Lancelot R 2012. aod: Analysis of Overdispersed Data. R package version 13. http://cran.r-project.org/package=aod.

Li CY, Tanaka M, Creutzfeldt OD. 1989. Attention and eye movement related activation of neurons in the dorsal prelunate gyrus (area DP). Brain Res. 496:307–313.

Livingstone MS, Vincent JL, Arcaro MJ, Srihasam K, Schade PF, Savage T. 2017. Development of the macaque face-patch system. Nat Commun. 8:14897.

Luhmann HJ, Martinez Millan L, Singer W. 1986. Development of horizontal intrinsic connections in cat striate cortex. Exp Brain Res. 63:443–448.

Lukaszewicz A, Savatier P, Cortay V, Giroud P, Huissoud C, Berland M, Kennedy H, Dehay C. 2005. G1 phase regulation, area-specific cell cycle control, and cytoarchitectonics in the primate cortex. Neuron. 47:353–364.

Markov NT, Ercsey-Ravasz MM, Ribeiro Gomes AR, Lamy C, Magrou L, Vezoli J, Misery P, Falchier A, Quilodran R, Gariel MA, et al. 2014. A weighted and directed interareal connectivity matrix for macaque cerebral cortex. Cereb Cortex. 24: 17–36.

Markov NT, Ercsey-Ravasz M, Van Essen DC, Knoblauch K, Toroczkai Z, Kennedy H. 2013. Cortical high-density counter-stream architectures. Science. 342:1238406.

Markov NT, Misery P, Falchier A, Lamy C, Vezoli J, Quilodran R, Gariel MA, Giroud P, Ercsey-Ravasz M, Pilaz LJ, et al. 2011. Weight consistency specifies regularities of macaque cortical networks. Cereb Cortex. 21:1254–1272.

Markov NT, Vezoli J, Chameau P, Falchier A, Quilodran R, Huissoud C, Lamy C, Misery P, Giroud P, Barone P, et al. 2014. The anatomy of hierarchy: feedforward and feedback pathways in macaque visual cortex. J Comp Neurol. 522:225–259.

Matteau I, Kupers R, Ricciardi E, Pietrini P, Ptito M. 2010. Beyond visual, aural and haptic movement perception: hMT+ is activated by electrotactile motion stimulation of the tongue in sighted and in congenitally blind individuals. Brain Res Bull. 82:264–270.

McCullagh P, Nelder JA. 1989. Generalized linear models. Boca Raton: Chapman & Hall/CRC.

Merabet LB, Pascual-Leone A. 2010. Neural reorganization following sensory loss: the opportunity of change. Nat Rev Neurosci. 11:44–52.

Michalareas G, Vezoli J, van Pelt S, Schoffelen JM, Kennedy H, Fries P. 2016. Alpha-beta and gamma rhythms subserve feedback and feedforward influences among human visual cortical areas. Neuron. 89:384–397.

Miyashita-Lin EM, Hevner R, Wassarman KM, Martinez S, Rubenstein JL. 1999. Early neocortical regionalization in the absence of thalamic innervation. Science. 285:906–909.

Molnar Z, Knott GW, Blakemore C, Saunders NR. 1998. Development of thalamocortical projections in the South American gray short-tailed opossum (Monodelphis domestica). J Comp Neurol. 398:491–514.

Moreno-Juan V, Filipchuk A, Anton-Bolanos N, Mezzera C, Gezelius H, Andres B, Rodriguez-Malmierca L, Susin R, Schaad O, Iwasato T, et al. 2017. Prenatal thalamic waves regulate cortical area size prior to sensory processing. Nat Commun. 8:14172.

Noppeney U, Friston KJ, Ashburner J, Frackowiak R, Price CJ. 2005. Early visual deprivation induces structural plasticity in gray and white matter. Curr Biol. 15:R488–R490.

Olavarria J, Van Sluyters RC. 1984. Callosal connections of the posterior neocortex in normal-eyed, congenitally anophtalmic, and neonatally enucleated mice. J Comp Neurol. 230: 249–268.

O'Leary DD, Chou SJ, Sahara S. 2007. Area patterning of the mammalian cortex. Neuron. 56:252–269.

O'Leary DD, Nakagawa Y. 2002. Patterning centers, regulatory genes and extrinsic mechanisms controlling arealization of the neocortex. Curr Opin Neurobiol. 12:14–25.

Pascual-Leone A, Hamilton R. 2001. The metamodal organization of the brain. Prog Brain Res. 134:427–445.

Pasqualotto A, Lam JS, Proulx MJ. 2013. Congenital blindness improves semantic and episodic memory. Behav Brain Res. 244:162–165.

Pietrini P, Furey ML, Ricciardi E, Gobbini MI, Wu WH, Cohen L, Guazzelli M, Haxby JV. 2004. Beyond sensory images: object-based representation in the human ventral pathway. Proc Natl Acad Sci USA. 101:5658–5663.

Polleux F, Dehay C, Kennedy H. 1997. The timetable of laminar neurogenesis contributes to the specification of cortical areas in mouse isocortex. J Comp Neurol. 385:95–116.

Polleux F, Dehay C, Kennedy H. 1998. Neurogenesis and commitment of corticospinal neurons in reeler. J Neurosci. 18: 9910–9923.

Pouchelon G, Gambino F, Bellone C, Telley L, Vitali I, Luscher C, Holtmaat A, Jabaudon D. 2014. Modality-specific thalamocortical inputs instruct the identity of postsynaptic L4 neurons. Nature. 511:471–474.

Pouchelon G, Jabaudon D. 2014. Nurturing the cortex's thalamic nature. Curr Opin Neurol. 27:142–148.

Ptito M, Matteau I, Gjedde A, Kupers R. 2009. Recruitment of the middle temporal area by tactile motion in congenital blindness. Neuroreport. 20:543–547.

R Development Core Team. 2016. R: A language and environment for statistical computing. Vienna, Austria: R Foundation for statistical computing. http://www.R-project.org.

Rakic P. 1974. Neurons in rhesus monkey visual cortex: systematic relation between time of origin and eventual disposition. Science. 183:425–427.

Rakic P. 1988. Specification of cerebral cortical areas. Science. 241:170–176.

Rakic P, Suner I, Williams RW. 1991. A novel cytoarchitectonic area induced experimentally within the primate visual cortex. Proc Natl Acad Sci USA. 88:2083–2087.

Reich L, Szwed M, Cohen L, Amedi A. 2011. A ventral visual stream reading center independent of visual experience. Curr Biol. 21:363–368.

Reveley C, Seth AK, Pierpaoli C, Silva AC, Yu D, Saunders RC, Leopold DA, Ye FQ. 2015. Superficial white matter fiber systems impede detection of long-range cortical connections in diffusion MR tractography. Proc Natl Acad Sci USA. 112: E2820–E2828.

Rhoades RW, Dellacroce DD. 1980. Neonatal enucleation induces an asymmetric pattern of visual callosal connections in hamsters. Brain Res. 202:189–195.

Roberts JA, Perry A, Lord AR, Roberts G, Mitchell PB, Smith RE, Calamante F, Breakspear M. 2016. The contribution of geometry to the human connectome. Neuroimage. 124:379–393.

Robinson SR, Dreher B. 1990. The visual pathways of eutherian mammals and marsupials develop according to a common timetable. Brain Behav Evol. 36:177–195.

Roder B, Stock O, Bien S, Neville H, Rosler F. 2002. Speech processing activates visual cortex in congenitally blind humans. Eur J Neurosci. 16:930–936.

Ruthazer ES, Cline HT. 2004. Insights into activity-dependent map formation from the retinotectal system: a middle-of-the-brain perspective. J Neurobiol. 59:134–146.

Sadato N, Pascual-Leone A, Grafman J, Ibanez V, Deiber MP, Dold G, Hallett M. 1996. Activation of the primary visual cortex by Braille reading in blind subjects. Nature. 380:526–528.

Selleck SB, Gonzalez C, Glover DM, White K. 1992. Regulation of the G1-S transition in postembryonic neuronal precursors by axon ingrowth. Nature. 355:253–255.

Shen Q, Wang Y, Dimos JT, Fasano CA, Phoenix TN, Lemischka IR, Ivanova NB, Stifani S, Morrisey EE, Temple S. 2006. The timing of cortical neurogenesis is encoded within lineages of individual progenitor cells. Nat Neurosci. 9:743–751.

Shimony JS, Burton H, Epstein AA, McLaren DG, Sun SW, Snyder AZ. 2006. Diffusion tensor imaging reveals white matter reorganization in early blind humans. Cereb Cortex. 16:1653–1661.

Shu N, Li J, Li K, Yu C, Jiang T. 2009. Abnormal diffusion of cerebral white matter in early blindness. Hum Brain Mapp. 30: 220–227.

Striem-Amit E, Cohen L, Dehaene S, Amedi A. 2012. Reading with sounds: sensory substitution selectively activates the visual word form area in the blind. Neuron. 76:640–652.

Striem-Amit E, Dakwar O, Reich L, Amedi A. 2012. The large-scale organization of "visual" streams emerges without visual experience. Cereb Cortex. 22:1698–1709.

Striem-Amit E, Ovadia-Caro S, Caramazza A, Margulies DS, Villringer A, Amedi A. 2015. Functional connectivity of visual cortex in the blind follows retinotopic organization principles. Brain. 138:1679–1695.

Sur M, Leamey CA. 2001. Development and plasticity of cortical areas and networks. Nat Rev Neurosci. 2:251–262.

Thomas C, Ye FQ, Irfanoglu MO, Modi P, Saleem KS, Leopold DA, Pierpaoli C. 2014. Anatomical accuracy of brain connections derived from diffusion MRI tractography is inherently limited. Proc Natl Acad Sci USA. 111:16574–16579.

Ungerleider LG, Galkin TW, Desimone R, Gattass R. 2008. Cortical connections of area V4 in the macaque. Cereb Cortex. 18:477–499.

van den Hurk J, Van Baelen M, Op de Beeck HP. 2017. Development of visual category selectivity in ventral visual cortex does not require visual experience. Proc Natl Acad Sci USA. 114:E4501–E4510.

van der Loos H, Dorfl J. 1978. Does the skin tell the somatosensory cortex how to construct a map of the periphery? Neurosci Lett. 7:23–30.

Van der Loos H, Woolsey TA. 1973. Somatosensory cortex: structural alteration following early injury to sense organs. Science. 179:395–398.

Venables WN, Ripley BD. 2002. Modern applied statistics with S. New York: Springer.

Vezoli J, Falchier A, Jouve B, Knoblauch K, Young M, Kennedy H. 2004. Quantitative analysis of connectivity in the visual cortex: extracting function from structure. Neuroscientist. 10: 476–482.

Watkins KE, Cowey A, Alexander I, Filippini N, Kennedy JM, Smith SM, Ragge N, Bridge H. 2012. Language networks in anophthalmia: maintained hierarchy of processing in 'visual' cortex. Brain. 135:1566–1577.

Wolbers T, Zahorik P, Giudice NA. 2011. Decoding the direction of auditory motion in blind humans. Neuroimage. 56:681–687.

Workman AD, Charvet CJ, Clancy B, Darlington RB, Finlay BL. 2013. Modeling transformations of neurodevelopmental sequences across mammalian species. J Neurosci. 33: 7368–7383.

Zembrzycki A, Perez-Garcia CG, Wang CF, Chou SJ, O'Leary DD. 2015. Postmitotic regulation of sensory area patterning in the mammalian neocortex by Lhx2. Proc Natl Acad Sci USA. 112:6736–6741.